RSC Advances

PAPER

View Article Online
View Journal | View Issue

Cite this: *RSC Adv.*, 2018, **8**, 16061

Morphology and mechanical behavior of diamond films fabricated by IH-MPCVD

Rong Tu,[a] Tiantian Xu,[a] Dengfeng Li,[a] Song Zhang,*[a] Meijun Yang,[a] Qizhong Li,[b] Lianmeng Zhang,[a] Toshihiro Shimada,[ac] Takashi Goto[ad] and Ji Shi[ae]

Received 3rd March 2018
Accepted 24th April 2018

DOI: 10.1039/c8ra01871e

rsc.li/rsc-advances

Morphology of diamond films has been controlled *via* intermediate frequency induction heated microwave plasma chemical vapor deposition (IH-MPCVD), which was transformed with various substrate temperatures (T_{sub} = 923–1123 K) and CH_4/H_2 ratios (η_c = 0.5–2 vol%). The coupling effects of T_{sub} and η_c on the structure of diamond films have been studied. At η_c = 0.5 vol%, the sp^3/sp^2 ratio of diamond films reached 98% at 1073 K, surface roughness (R_{ms}) increased from 50 to 85 nm with increasing T_{sub}, the maximum hardness (H_a) reached 84 GPa at 973 K, and the maximum Young's modulus (E) reached 642 GPa at 1023 K. The residual stress (σ) was calculated as a function of T_{sub} and η_c. The quality factor (Q), combining microstructure and mechanical behavior, has been creatively defined to evaluate the quality of diamond films.

1. Introduction

Chemical vapor deposited (CVD) diamond covers a broad range of synthetic diamond materials with great variety of properties such as high hardness, high elastic modulus, chemical inertness, and low self-friction coefficient.[1–4] CVD diamond can be broadly divided into two grades, *i.e.*, microcrystalline diamond (MCD) and nanocrystalline diamond (NCD), with the crystallites in the micron size range and smaller than 500 nm, respectively.[5] NCD films are highly desirable for the substrates of MEMS (Micro-Electro-Mechanical Systems) because the smaller grain size insures a smoother surface for the devices above comparing with MCD.[6–8] However, the mechanical properties of NCD, such as hardness and elastic modulus, are lower than those of conventional MCD due to the presence of sp^2 non-diamond species.[9] Therefore, the smooth surface, good mechanical property and high sp^3/sp^2 ratio are usually difficult to obtain simultaneously, and it is hard to evaluate the quality of diamond-related materials only according to their individual properties. Here, we define quality factor (Q), combining microstructure and mechanical behavior to evaluate the deposits.

Besides, substrate temperature (T_{sub}) plays an important role in growth process of diamond. Not only the structure and properties of CVD diamond films, but also the growth rate is mainly influenced by T_{sub}. For example, the commonly low T_{sub} may hinder the formation of strong chemical bonds between atoms, while the high temperature may enhance the graphite species.[10] However, it is difficult to control precisely the T_{sub} in MPCVD system because the T_{sub} is attributed to several factors, *e.g.*, discharging plasma density and substrate location, which is influenced strongly by the microwave power (p_w). Moreover, T_{sub} would certainly decrease due to the heat exchange between the chamber and external environment. And it is hard to increase the decreased T_{sub} by adjusting p_w due to its strong influence on T_{sub}. In general, T_{sub} is difficult to be precisely controlled only through the adjustment of p_w, which resulting in the difficulty of researches on diamond structures.

In this study, an IH-MPCVD apparatus was developed to fabricate diamond films. The T_{sub} was compensated with an intermediate frequency induction heating system by self-adjusting the IH power (p_h) according to the thermocouple that set under the substrate. The effects of CH_4/H_2 ratio and deposition temperature on the morphology, quality factor (Q) and deposition rate of the diamond films has been investigated, and the growth mechanism of these films was also proposed.

2. Experimental

Fig. 1 shows the experimental schematic of the home-made induction heated microwave plasma CVD (IH-MPCVD). The system consisted of a microwave generator network (MPS-15D, NISSIN, Tokyo, Japan, 2.45 GHz, 1.5 kW), a quartz tube chamber, an intermediate frequency induction heating device

[a]State Key Laboratory of Advanced Technology for Materials Synthesis and Processing, Wuhan University of Technology, 122 Luoshi Road, Wuhan 430070, People's Republic of China. E-mail: kobe@whut.edu.cn; superkobe0104@gmail.com
[b]Hubei Key Laboratory Advanced Technology of Automobile Parts, Wuhan University of Technology, 122 Luoshi Road, Wuhan 430070, People's Republic of China
[c]Division of Applied Chemistry, Hokkaido University, Sapporo 060-0808, Japan
[d]Institute for Materials Research, Tohoku University, 2-1-1 Katahira, Aoba-ku, Sendai 980-8577, Japan
[e]Japan Department of Metallurgy and Ceramics Science, Tokyo Institute of Technology, Tokyo 152-8552, Japan

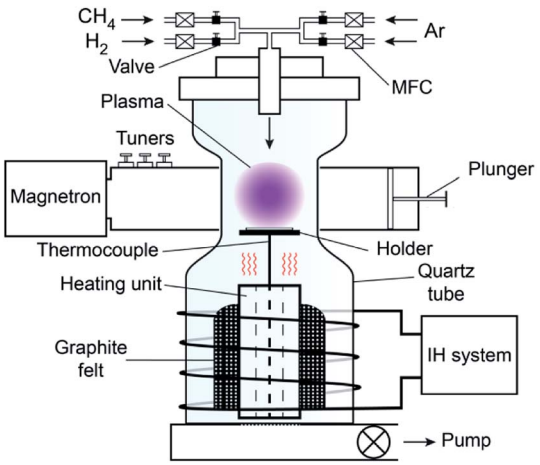

Fig. 1 Schematic diagram of the IH-MPCVD system.

(S08-6093, Daiichi Kiden, Tokyo, Japan, 6 kHz, 12.5 kW), and a vacuum system. A hollow graphite cylinder heated by the induction heating device was set below the substrate holder as heating unit surrounded by a graphite felt. The substrate holder was supported by an alumina tube within a K-type thermocouple. The temperature signals of thermocouple were fed back to the IH-system.

Single-crystalline silicon ⟨100⟩ wafers with dimensions of 10.0 × 15.0 × 0.5 mm were used as substrates. To enhance nucleation, the Si substrates were scratched *via* ultrasonic bath in acetone with diamond powders (10–40 μm) for 1 hour. The scratched substrates were taken ultrasonic cleaning in deionized water, and then dried in a N_2 flow.

The substrates were preheated at 873 K in 30 minutes after quartz chamber was evacuated to 10^{-1} Pa. The input gas flow rate of H_2 (f_h) was 400 sccm. The flow rate of CH_4 (f_c) was varied from 1 to 10 sccm. The total pressure (P_{tot}) and the microwave power (p_w) were 4 kPa and 900 W, respectively. The induction heating power (p_h) of the intermediate frequency induction heating device was self-adjusted from 0 to 12.5 kW, according to the substrate temperature assessed by thermocouple. Thus, the substrate temperatures (T_{sub}) were controlled in the range of 923–1123 K. The depositions for all samples were carried out for a total time of 3 h.

Phase identification of the films was obtained by Raman spectra (LabRAM HR Evolution; Horiba, Paris, France) with the excitation of a diode laser 532 nm in wavelength. Crystalline phases were examined by X-ray diffraction with Cu-Kα radiation (XRD; Ultima III, Rigaku, Tokyo, Japan, at 40 kV and 40 mA). A field-emission scanning electron microscope (SEM; Quanta-250, FEI, Houston, TX, at 20 kV) was used to observe the film thickness and microstructure. The surficial roughness was analyzed by atomic force microscopy (AFM; Multimode 8-HR, Bruker, Santa Barbara, USA). The hardness and young's modulus were analyzed by a MTS Nano-indenter (Agilent Technologies G200, California, USA).

3. Results and discussion

Fig. 2(a)–(e) shows the surficial morphology of diamond films grown at T_{sub} = 1073 K and various CH_4/H_2 ratio (η_c) ranging from 0.5 to 2.5 vol%. At η_c = 0.5%, the film consisted of regulated quadrate grains with average size of 0.36 μm [Fig. 2(a)]. At η_c = 1.0% and 1.5%, the films exhibited faceted columnar structure with average grain size of 0.34 μm and 0.44 μm, respectively [Fig. 2(b and c)]. At η_c = 2.0%, the grains were coated by nanoparticles [Fig. 2(d)]. By increasing η_c to 2.5%, the films showed dense spherical "cauliflower-like" morphology [Fig. 2(e)]. The cauliflower-like structures was also observed by Hemawan[11] *via* AP-MPCVD. They explained that the formation of spherical and polygonal shapes in the atmospheric pressure MPCVD was due to surface diffusion and condensation from vapor phase.[12] The cross-sectional view [Fig. 2(f–j)] revealed the film thickness reached the maximum at η_c = 1.5%.

The minimum roughness (R_{ms}) of film surface is approximately 23.4 nm at η_c = 2.0–2.5%, as shown in Fig. 3, which is much smaller than that obtained at low η_c = 1.0% (about 80 nm). Fig. 4 shows the XRD patterns of the deposit, the peaks corresponding to diamond (111) at 43.9° (2θ) were only detected for all the specimens, indicating (111) orientation. In terms of

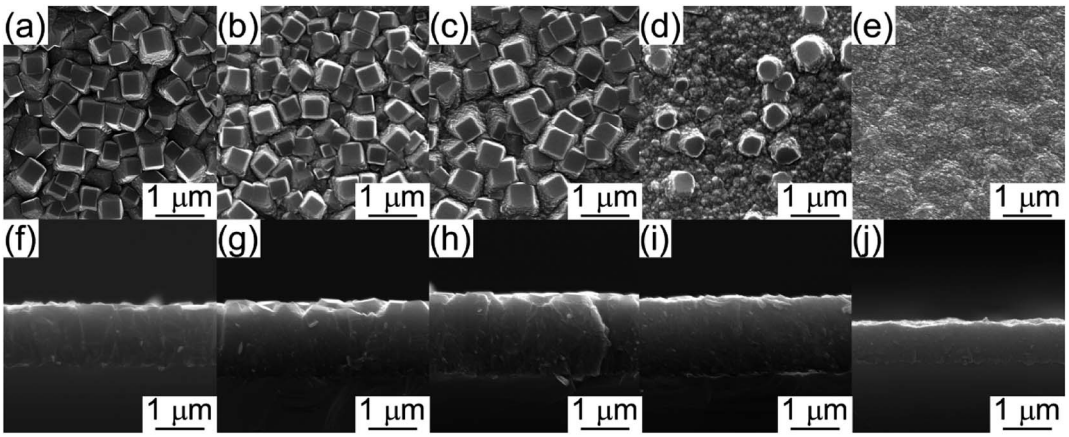

Fig. 2 Surficial and cross-sectional SEM image of diamond films deposited at T_{sub} = 1073 K and various CH_4/H_2 ratio (η_c): (a and f) 0.5, (b and g) 1.0, (c and h) 1.5, (d and i) 2.0 and (e and j) 2.5 vol%.

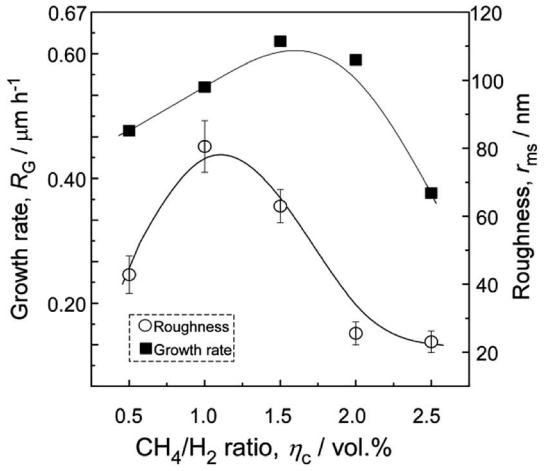

Fig. 3 Effect of η_c on the surface roughness and growth rate of the diamond films at $T_{sub} = 1073$ K.

carbon chemistry in the plasma discharge, relatively higher η_c results in rich [C_xH_y] and other methyl radicals which are important for diamond nucleation. These species enhance the re-nucleation process of diamond, as well as the sp^2 hybridized carbon formation.[13] By reducing the CH_4 fraction in the plasma, the C_xH_y species decreased, especially the species with $x > 3$ (*e.g.* [C_4H_2], [C_3H_2]). As a result, the hydrocarbon species with $x \leq 2$ incorporates into the lattice by forming a C–C bond to an atom that belongs to a lower-lying terrace, and weaken the nucleation of sp^2 hybridized carbon phase.[5] Therefore, well-faceted diamond prefers relatively lower η_c under a constant microwave power in this study.

Fig. 5 shows the cross-sectional and surficial SEM image of diamond films deposited at various T_{sub} ranging from 923 to 1123 K at $\eta_c = 0.5\%$. The cross-sectional images revealed that the film thickness varied from 0.5 to 1.9 μm [Fig. 5(f)–(j)]. Namely, in this range, the substrate temperature caused an enhancement in diamond growth rate (R_G).

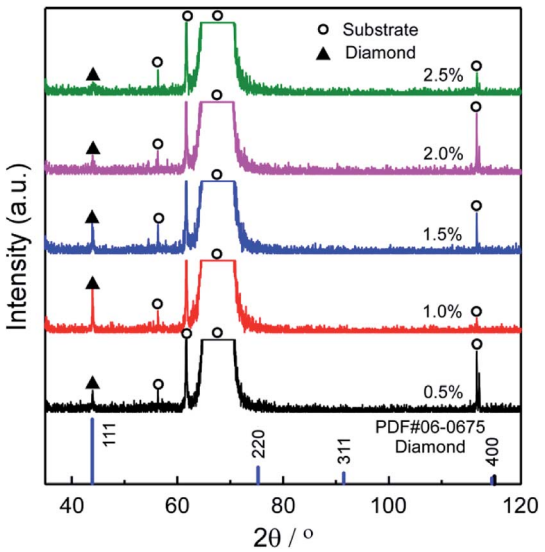

Fig. 4 XRD patterns of films deposited at $T_{sub} = 1073$ K and various η_c.

The magnified details of the samples are given in Fig. 5(a)–(e), pyramidal micrometric diamond crystals are visible at the terminal surface, both triangular and square facets corresponding to {111} and {100} lattice plane were observed. The quadrate planes of {100} facets appear at all the samples [Fig. 5(a–e)], while the triangular {111} facets present at lower temperature [Fig. 5(a–c)]. Area ratio of square and triangular planes obviously grew larger with the increasing of T_{sub} (923–1073 K), owing to the different growth ratio (R_{hkl}) of each plane. According to the Wulff configurations,[14] the slowest growing plane would be the one survive in growing diamond particles, and *vice versa*, the fastest one would disappear completely. Fig. 5(k–n) illustrate the Wulff configurations for diamond deposited at 923, 973, 1023, 1073 K respectively as a function of the facet growth ratio of {100} over {111}, defined as parameter α. The XRD result of this group sample shows that only diamond (111) at 43.9° (2θ) was detected, indicating (111) orientation.

Wild *et al.*[15] introduced the growth parameter α which relates the growth rates along different crystal axes; ⟨111⟩ direction would be the fastest growing direction when α is 1, and the growth morphology would be cubic; when α is 3, the fastest growing direction would be ⟨100⟩ direction, and the growth morphology would be octahedron. For example, in addition to the twinning process, the CVD diamond would show truncated octahedron morphology in various scale when α is 1.5. In this study, for diamond deposited at 923–1023 K [Fig. 5(k)–(m)], α is 1 to 3, and α increase with T_{sub}. For diamond deposited at 1073 K [Fig. 5(n)], α is close to 3. In conclusion, the parameter α shows a negative relation with the rising T_{sub}, indicating that the R_{111} increases faster than the R_{100} with the T_{sub} [Fig. 5(a)–(d)].

Others have reported the order of calculated energy barriers of different diamond surface planes (*i.e.* {110} < {111} < {100}).[16–19] Namely, {100} surface planes are the most stable facets of CVD diamond grains among H-rich plasma, and the hydrogen abstraction process on {111} facets run faster than those on {100} facets. The whole growth process of CVD diamond would speed up with increasing T_{sub}, as a result, the growth rate of ⟨111⟩ direction would be much faster than ⟨100⟩ direction.

Fig. 6 shows the surficial roughness increased with increasing T_{sub} except one grown at 1123 K and accompanied by an increasing of film thickness and grain size. These findings are understandable because the diamond film presents a columnar crystal cross-section in Fig. 5, which indicates that the evolution of grain size follows the van der Drift model[14] with columnar structure. The diagram in Fig. 6 depicts the evolution of film thickness and surficial roughness in this temperature series.[6,20,21] The surficial roughness and film thickness showed a positive correlation, except one grown at 1123 K. The AFM topographies suggest that the spherical carbon species may present at higher T_{sub}, and these amorphous little particles prefer to generate at the ravines between the micro-crystalline grains, which slightly decrease the roughness.

Fig. 7 shows the dependence of the R_G on the T_{sub}. The R_G of diamond films, with a good quality, is at an intermediate level.

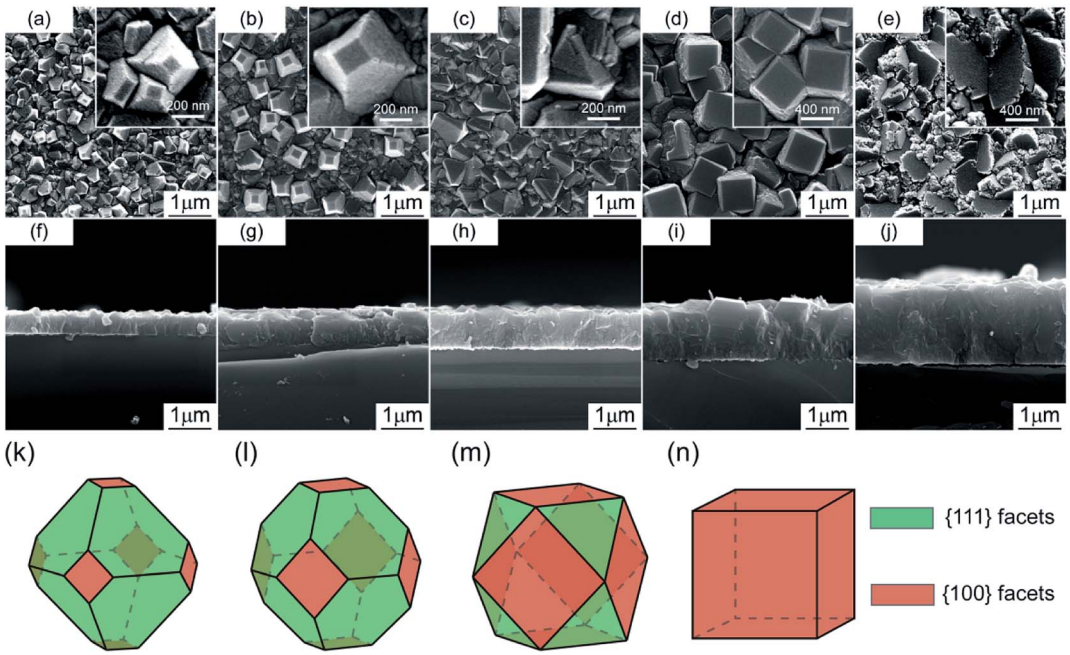

Fig. 5 Cross-sectional and surficial SEM image of diamond films deposited at T_{sub} = 923 (a and f), 973 (b and g), 1023 (c and h), 1073 (d and i) and 1123 K (e and j) and η_c = 0.5 vol%. (k–n) is the Wulff configurations for diamond as a function of the facet growth ratio of {100} over {111}.

The activation energy of 53 kJ mol^{-1} calculated by Arrhenius plot of the R_G *versus* a reciprocal T_{sub}. The result indicates that diamond growth process is limited by temperature controlled chemical process, which under a constant microwave power. Stiegler *et al.*[25] investigated the growth kinetics of diamond films deposited at low substrate temperatures (673–873 K), and they supposed that increasing R_G is most probably caused by the removal of surface bonded hydrogen atoms from the carbon sites. Thus, we induced that with a higher temperature, the removal of surface bonded hydrogen atoms would get easier, and then caused a higher R_G.

Fig. 8 indicates the Raman spectra for the films deposited at different T_{sub}. In all samples, a sharp peak has been observed at 1332 cm^{-1}, which corresponds to the zone center of T_{2g} symmetry of diamond. The other obvious characteristic peak occurs at 1575 cm^{-1} presenting the zone center E_{2g} mode of crystalline graphite, and it is usually designated as the "G" band for graphite. Besides, in micro-crystalline graphite, an additional sharp peak should appear at a wave number of 1350 cm^{-1} in the Raman spectra, which represents a zone-edge A_{1g} mode, named "D" band.[27,28] However, the peak of "D" band, which close to the sharp diamond T_{2g} peak, was absent from all the Raman spectra in Fig. 8. Namely, there is little crystalline graphite in these diamond films. In addition to the diamond and graphite, for all the other kinds of amorphous and nanocrystalline carbon species, the Raman spectra typically shows a shoulder and broad "G" band centered around 1550 cm^{-1} and a "D" band centered at 1375 cm^{-1}.[29] The intensity of sharp diamond peak is much higher than the other peaks, which indicates the higher proportion of sp^3 carbon atoms in these samples. With increasing T_{sub}, the related intensity of broad G peak increases, and the "G" band slightly moves up to 1580 cm^{-1}. The slight shift in the broad "G" band frequency is consistent with an increase of amorphous component which produced from the carbon soot formation.[30] The downshift and broadening of the diamond peak in nanocrystalline diamond also have previously been observed and explained by quantum confinement effect.[31] The phase purity is evaluated by the sp^3/sp^2 ratio (r) from the Raman spectra and expressed as eqn (1),[32]

$$r = \frac{75 \times I_d}{75 \times I_d + \sum_{nd} I_{nd}} \times 100\% \quad (1)$$

where, I_d is the Raman diamond peak area centered at 1332 cm^{-1} and $\sum_{nd} I_{nd}$ is the sum of Raman sp^2 phase peak areas. The

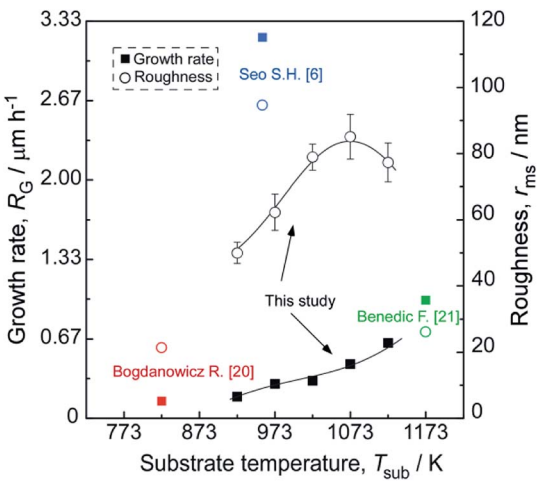

Fig. 6 Evolution of the surface roughness and growth rate of the diamond films synthesized at various T_{sub}, η_c = 0.5 vol%.

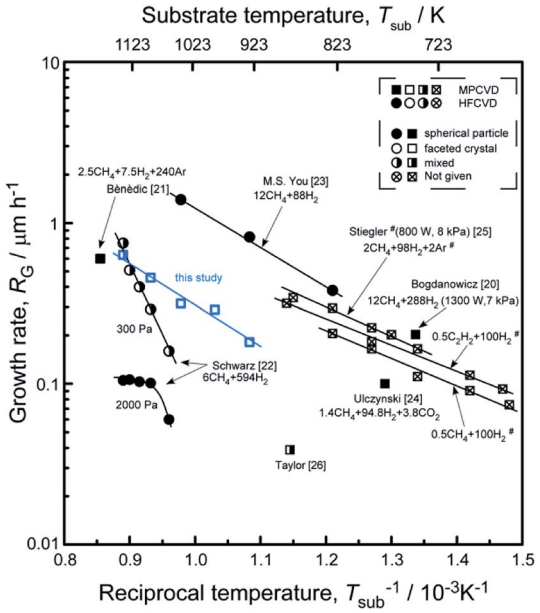

Fig. 7 Effect of T_{sub} on R_G, η_c = 0.5 vol%.

factor 75 takes into account the more effective Raman scattering of sp^2 structures.[33,34] The sp^3/sp^2 ratio of samples shown in Fig. 8 are various from 93 to 98%. However, it should be noticed that two weak peaks occur at 1140 cm^{-1} and 1450 cm^{-1}, respectively. Others have reported the two peaks not only appear together, yet they also show quite strong and similar dispersions, while the diamond mode does not. Moreover, Kuzmany *et al.*[35] have given a clear proof that these peaks originate from *trans*-polyacetylene in the grain boundaries by the H–D isotopic substitution result. In Raman features observed here, these two peaks usually occur in the Raman spectra of samples deposited at low temperatures. This is due to the slow growth rate at low T_{sub}, and the re-nucleating process leads to a high nucleation

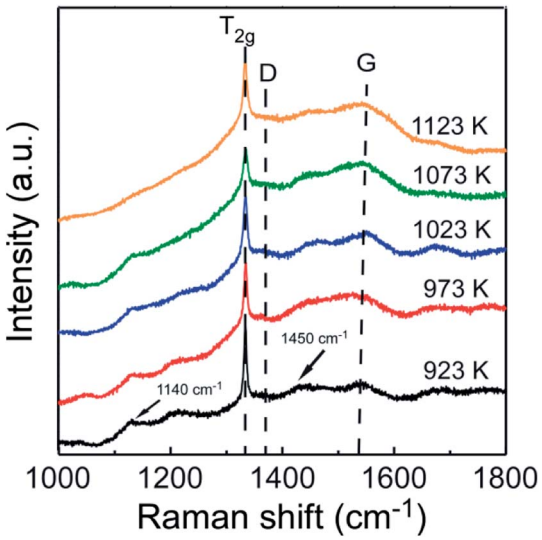

Fig. 8 Raman spectra of the diamond films synthesized at various T_{sub}, η_c = 0.5 vol%.

density with a large amount of boundaries among little grains, where polyacetylene existed. In order to ensure the quality of diamond films, the T_{sub} during diamond growth process should not be higher than 1073 K, neither be lower than 973 K in this study.

As shown in Fig. 9, the surficial morphologies of diamond films can be defined as three categories: the well-faceted crystalline, the spherical structures composited with nanoparticles, and the mixture of both morphologies. At a relative high T_{sub} (≥1073 K), {100} planes occurred on the film surface. For high CH_4/H_2 ratio ($\eta_c \geq 2.0\%$) and low T_{sub} (≤973 K), more spherical nanoparticles were formed instead of crystalline structure.

In order to follow the mechanical properties, a nano-indentation technique was performed. Fig. 10 demonstrates the relationships between average hardness (H_a), Young's modulus (E) and T_{sub}. The H_a and E were calculated from the correlation between load/unload and displacement (*i.e.*, displacement–load curves not shown here). The theoretical value of Poisson's coefficient (ν) used for calculating the Young's modulus was 0.20, according to the Poisson's ratio of CVD polycrystalline diamond.[36] The results reveal that the H_a and E of films increased with T_{sub} when it ranged in 923–1073 K; the maximum H_a and E reached 84 GPa at 973 K and 642 GPa at 1023 K, respectively. The value is twice as much as regular NCD films by MPCVD,[37] much hard than those deposited in argon plasma.[38] Exceptionally, both H_a and E decreased marginally when T_{sub} beyond 1123 K. This anomaly may result from non-diamond phases generated among diamond crystals, confirmed by SEM, AFM and Raman spectra.

For most applications of diamond films, such as wear-resistant coatings, heatsinks, MEMS and surface acoustic wave devices, a high sp^3 component, a high hardness and a low surface roughness are crucial and favorable, but are hard to possess simultaneously. For example, diamond film with an extreme smooth surface always shows a poor mechanical property and low sp^3/sp^2 ratio. To evaluate the quality of different diamond films by microstructure and mechanical behaviors, we proposed a parameter, quality factor (Q), as a formula model:

$$Q = \frac{r^a \times H^b}{R_{ms}{}^c} \quad (2)$$

where, r refers to sp^3/sp^2 ratio, H refers to hardness, R_{ms} refers to surface roughness, a, b, c are exponential parameters, Q refers to the quality factor of diamond films, the higher the value of Q, the better the quality of diamond films. This formula model is reasonable from a qualitative point of view, because a high r and H, and a low R_{ms} result in a high value of Q, which means a high quality of diamond film, accordingly, a high sp^3 component and hardness, and a low surface roughness are favourable for most applications of diamond films. Here, values of a, b, c were provided as 4, 4, 0.5 respectively, based on the researches in this study after fitting.

Fig. 11 shows Q of DLC,[39] NCD[40] and diamond[41] materials fabricated at different conditions ($p_w \times \eta_c \times P_{tot}$), in which DLC, NCD and diamond area are classified by Q in the order of 1 × 10^4, 1 × 10^5 and 1 × 10^6, respectively. Through comparing the

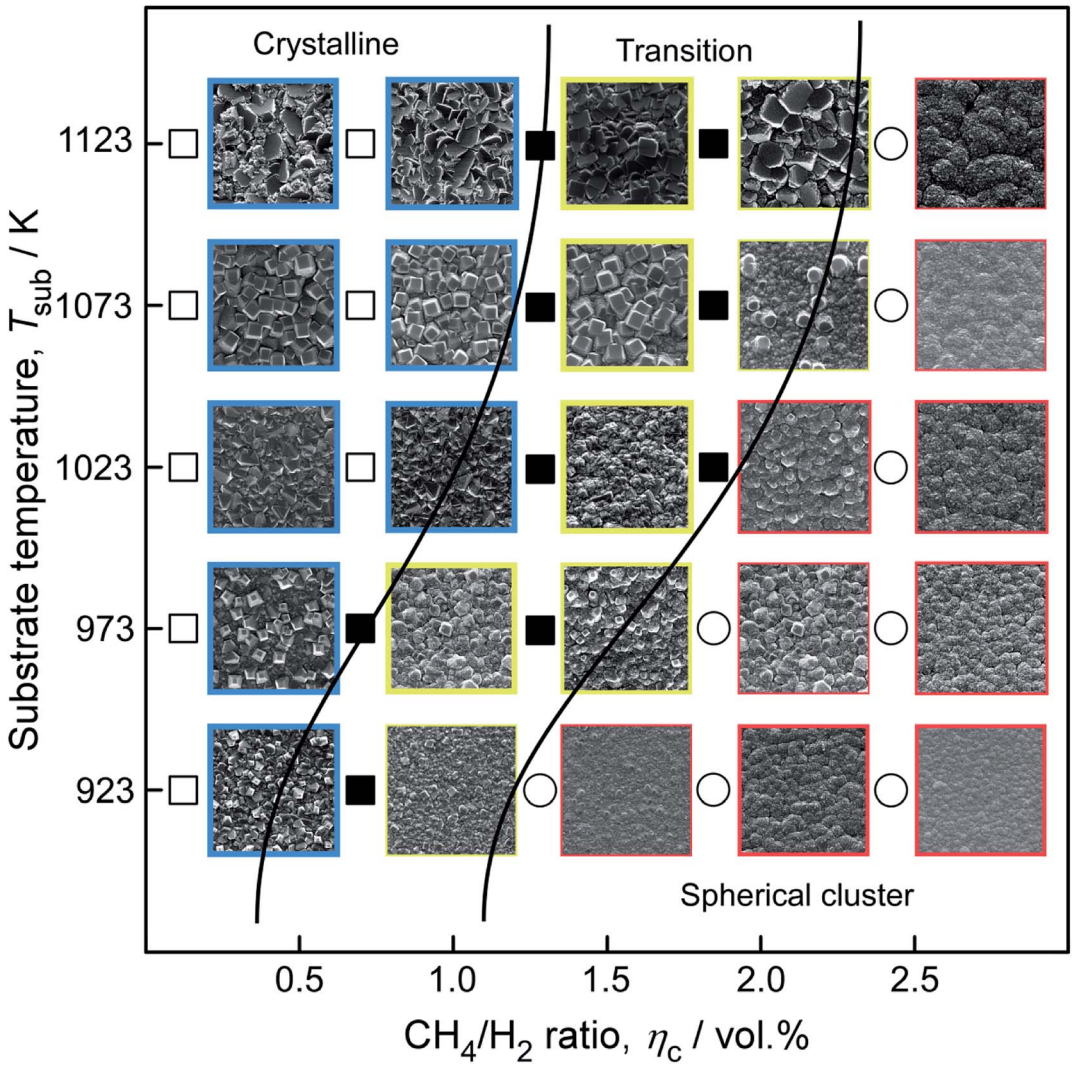

Fig. 9 Coupling effects of η_c and T_{sub} on structure of diamond films.

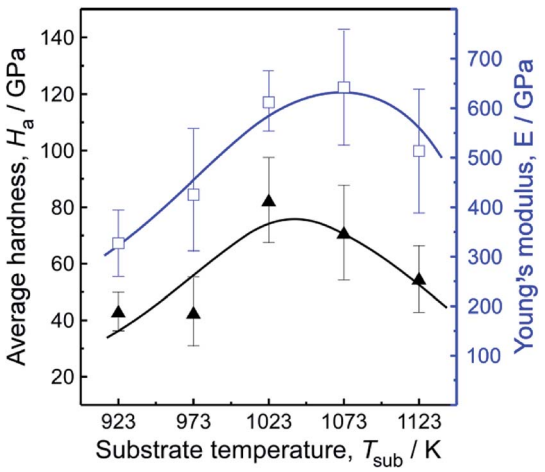

Fig. 10 Average hardness (H_a) and Young's modulus (E) of samples fabricated with various T_{sub}, η_c = 0.5 vol%.

values of Q, we could judge the quality of the diamond related materials more visually. Most specimens fabricated in this study are in the diamond area and NCD area, which demonstrates that with a relatively good quality, the diamond films in the present study would have a good performance in wear-resistant coatings, heatsinks, MEMS and surface acoustic wave devices.

The residual stress (σ), as a function of various T_{sub} at $\eta_c = 0.5\%$ and various η_c at 1073 K was calculated by eqn (3).[42]

$$\sigma = -0.567(\nu - \nu_0)\ (\text{GPa}) \quad (3)$$

where $\nu_0 = 1332\ \text{cm}^{-1}$, ν is the observed Raman shift corresponding to diamond peak, $\sigma < 0$ and $\sigma > 0$ correspond to the compressive and tensile stress, respectively. The residual stress generally includes intrinsic stress and thermal stress. The thermal stress is due to different thermal expansion coefficients of the film and substrate. Peng *et al.*[43] demonstrated that the intrinsic compressive stress of diamond films was mainly caused by impurities such as sp^2 bonded carbon and hydrogen,

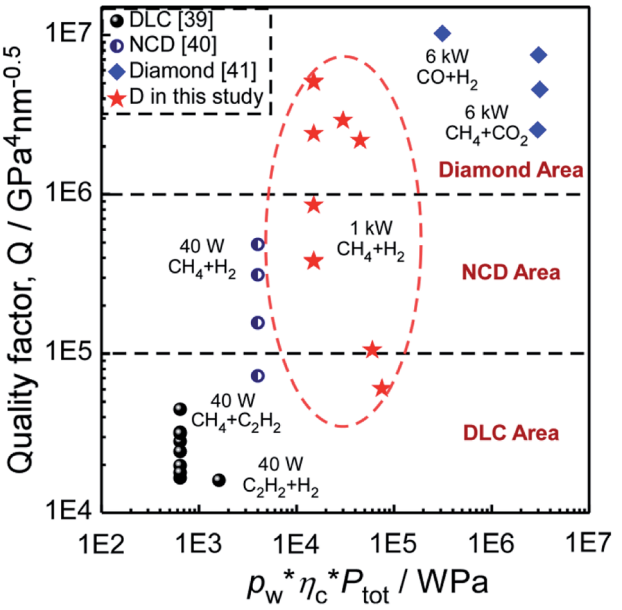

Fig. 11 Quality factor (Q) of DLC, NCD and Diamond materials fabricated at different conditions ($p_w \times \eta_c \times P_{tot}$).

and tensile stress was caused by defects such as excess vacancies, which mainly formed from sp^2 carbon after etching by atomic hydrogen, and grain boundaries.[44] Besides, the thicker of diamond film, the higher of the compressive stress.[45] As shown in Fig. 12, σ increased from −1.54 to −0.79 GPa as T_{sub} increased from 923 K to 1073 K, which was ascribed to decreasing sp^2 bonded carbon content with T_{sub}. However, a decrease of σ was observed at 1123 K due to the presence of spherical carbon species, and increase of film thickness as evidenced by SEM photograph in Fig. 5(e)–(j). With η_c increasing from 0.5 to 2.5%, σ increased from −0.79 to 0.60 GPa. Higher sp^2 carbon content was formed at higher η_c, most of which was etched away by atomic hydrogen and then

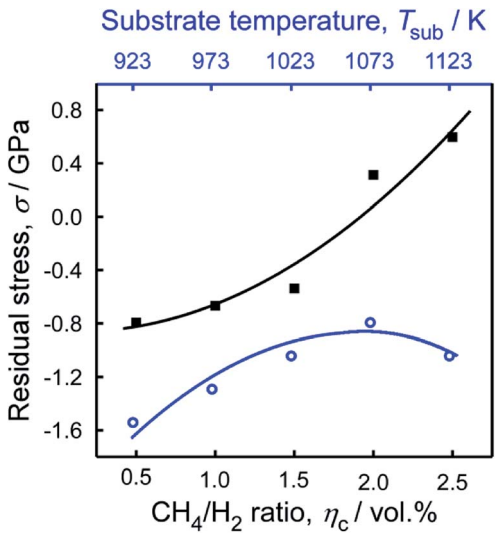

Fig. 12 Residual stress variation with T_{sub} (η_c = 0.5%) and η_c (T_{sub} = 1073 K).

became vacancies. The increasing excess vacancies produced tension stress and caused an increase in residual stress. Furthermore, nanocrystalline diamond preferred to grow at relatively higher η_c, as evidenced by SEM photograph in Fig. 2(d and e), resulting in an increase in density of grain boundaries, thus, σ increased.

4. Conclusions

To improve the thermal control process of MPCVD technique, we have explored an intermediate-frequency induction heated MPCVD (IH-MPCVD) system. Coupling effects of T_{sub} (923–1123 K) and η_c (0.5–2 vol%) on structure of diamond films shows that the surficial morphologies of diamond films can be defined as three categories: the well-faceted crystalline, the spherical structures composited with nanoparticles, and the mixture of both morphologies. Higher η_c (2.5 vol%) enhances the re-nucleation process which leads to a smooth surface, yet lower η_c (0.5 vol%) results in better crystalline quality of diamond films. At η_c = 0.5 vol%, the morphology transformed from pyramid to quadrate column with T_{sub} increasing from 923 to 1073 K, besides, the maximum hardness (H_a) and Young's modulus (E) was 84 GPa and 642 GPa, at T_{sub} = 1023, 1073 K, respectively. The residual stress increased from −1.54 to −0.79 GPa with T_{sub}, at η_c = 0.5 vol%, and then decreased, while at 1073 K, it increased with η_c and reached to 0.60 GPa at η_c = 2.5 vol%.

Conflicts of interest

There are no conflicts to declare.

Acknowledgements

This work was supported by the National Natural Science Foundation of China (No. 51372188, and 51521001) and by the 111 Project (B13035). This research was also supported by the International Science & Technology Cooperation Program of China (2014DFA53090) and the Natural Science Foundation of Hubei Province, China (2016CFA006), and the National Key Research and Development Program of China (2017YFB0310400), and the Fundamental Research Funds for the Central Universities (WUT: 2017II43GX, 2017III032, 2017YB004, 2018III016), and Science Challenge Project (No. TZ2016001).

References

1 F. A. Almeida, E. Salgueiredo, F. J. Oliveira, R. F. Silva, D. L. Baptista, S. B. Peripolli and C. A. Achete, *ACS Appl. Mater. Interfaces*, 2013, **5**, 11725.
2 J. J. Gracio, Q. H. Fan and J. C. Madaleno, *J. Phys. D: Appl. Phys.*, 2010, **43**, 374017.
3 R. S. Balmer, J. R. Brandon, S. L. Clewes, H. K. Dhillon, J. M. Dodson, I. Friel, P. N. Inglis, T. D. Madgwick, M. L. Markham, T. P. Mollart, N. Perkins, G. a. Scarsbrook,

D. J. Twitchen, a. J. Whitehead, J. J. Wilman and S. M. Woollard, *J. Phys.: Condens. Matter*, 2009, **21**, 364221.
4 A. Gicquel, K. Hassouni, F. Silva and J. Achard, *Curr. Appl. Phys.*, 2001, **1**, 479.
5 M. Eckert, E. Neyts and A. Bogaerts, *Cryst. Growth Des.*, 2010, **10**, 4123.
6 S. H. Seo, W. C. Shin and J. S. Park, *Thin Solid Films*, 2002, **416**, 190.
7 W. C. Shih, M. J. Wang and I. Nan Lin, *Diamond Relat. Mater.*, 2008, **17**, 390.
8 Y. Q. Fu, L. Garcia-Gancedo, H. F. Pang, S. Porro, Y. W. Gu, J. K. Luo, X. T. Zu, F. Placido, J. I. B. Wilson, A. J. Flewitt and W. I. Milne, *Biomicrofluidics*, 2012, **6**, 024105.
9 S. A. Catledge, J. Borham, Y. K. Vohra, W. R. Lacefield, J. E. Lemons, S. A. Catledge, J. Borham and Y. K. Vohra, *J. Appl. Phys.*, 2002, **91**, 5347.
10 O. A. Williams, M. Daenen, J. D'Haen, K. Haenen, J. Maes, V. V Moshchalkov, M. Nesládek and D. M. Gruen, *Diamond Relat. Mater.*, 2006, **15**, 654.
11 K. W. Hemawan, H. Gou, R. J. Hemley, K. W. Hemawan, H. Gou and R. J. Hemley, *Appl. Phys. Lett.*, 2015, **107**, 181901.
12 J. Kim, H. Sakakita, H. Ohsaki and M. Katsurai, *Jpn. J. Appl. Phys.*, 2015, **54**, 01AA02.
13 H. J. Lee, K. S. Lee, J. M. Cho, T. S. Lee, I. Kim, D. S. Jeong and W. S. Lee, *ACS Appl. Mater. Interfaces*, 2013, **5**, 11631.
14 A. Van der Drift, *Philips Res. Rep.*, 1967, **22**, 267.
15 C. Wild, R. Kohl, N. Herres, W. Müller-Sebert and P. Koidl, *Diamond Relat. Mater.*, 1994, **3**, 373.
16 J. Bühler and Y. Prior, *J. Cryst. Growth*, 2000, **209**, 779.
17 Y. Zou and K. Larsson, *J. Phys. Chem. C*, 2016, **120**, 10658.
18 K. E. Spear and J. P. Dismukes, in *Synthetic Diamond*, Wiley, New York, 1994, p. 663.
19 B. T. Van Regemorter and K. Larsson, *Chem. Vap. Deposition*, 2008, 224.
20 R. Bogdanowicz, M. Sobaszek, J. Ryl, M. Gnyba, M. Ficek, Ł. Gołuński, W. J. Bock, M. Śmietana and K. Darowicki, *Diamond Relat. Mater.*, 2015, **55**, 52.
21 F. Bénédic, M. B. Assouar, F. Mohasseb, O. Elmazria, P. Alnot and A. Gicquel, *Diamond Relat. Mater.*, 2004, **13**, 347.
22 S. Schwarz, S. M. Rosiwal, M. Frank, D. Breidt and R. F. Singer, *Diamond Relat. Mater.*, 2002, **11**, 589.
23 M. S. You, F. C. N. Hong, Y. R. Jeng and S. M. Huang, *Diamond Relat. Mater.*, 2009, **18**, 155.
24 M. J. Ulczynski, B. Wright and D. K. Reinhard, *Diamond Relat. Mater.*, 1998, **7**, 1639.
25 J. Stiegler, T. Lang, Y. Von Kaenel, J. Michler, E. Blank, J. Stiegler, T. Lang, Y. Von Kaenel, J. Michler and E. Blank, *Appl. Phys. Lett.*, 2014, **173**, 88.
26 A. Taylor, L. Fekete, P. Hubík, A. Jäger, P. Janíček, V. Mortet, J. Mistrík and J. Vacík, *Diamond Relat. Mater.*, 2014, **47**, 27.
27 P. K. Chu and L. Li, *Mater. Chem. Phys.*, 2006, **96**, 253.
28 T. S. Yang, J. Y. Lai, C. L. Cheng and M. S. Wong, *Diamond Relat. Mater.*, 2001, **10**, 2161.
29 S. Ray, A. R. Middya and A. K. Barua, *Jpn. J. Appl. Phys.*, 1993, **32**, L1559.
30 M. A. Pimenta, G. Dresselhaus, M. S. Dresselhaus, L. G. Cancado, A. Jorio and R. Saito, *Phys. Chem. Chem. Phys.*, 2007, **9**, 1276.
31 S. Osswald, V. N. Mochalin, M. Havel, G. Yushin and Y. Gogotsi, *Phys. Rev. B*, 2009, **80**, 75419.
32 F. Silva, A. Gicquel, A. Tardieu, P. Cledat and T. Chauveau, *Diamond Relat. Mater.*, 1996, **5**, 338.
33 J. R. Moro, *J. Mater. Sci.*, 2007, **42**, 7331.
34 R. E. Shroder, R. J. Nemanich and J. T. Glass, *Phys. Rev. B*, 1990, **41**, 3738.
35 H. Kuzmany, R. Pfeiffer, N. Salk and B. Günther, *Carbon*, 2004, **42**, 911.
36 C. A. Klein and G. F. Cardinale, *Diamond Relat. Mater.*, 1993, **2**, 918.
37 W. Kulisch, C. Popov, V. Vorlicek, P. N. Gibson and G. Favaro, *Thin Solid Films*, 2006, **515**, 1005.
38 Y. Wubao, K. Xiang, Y. Size and D. Xiaofeng, *Vacuum*, 2003, **68**, 49.
39 J. S. Hsu, S. S. Tzeng and Y. J. Wu, *Vacuum*, 2008, **83**, 622.
40 T. Sharda, T. Soga, T. Jimbo and M. Umeno, *J. Nanosci. Nanotechnol.*, 2001, **1**, 287.
41 M. I. De Barros, L. Vandenbulcke, L. Chinsky, D. Rats and J. Von Stebut, *Diamond Relat. Mater.*, 2001, **10**, 337.
42 J. R. Moro, *J. Mater. Sci.*, 2007, **42**, 7331.
43 X. L. Peng, Y. C. Tsui and T. W. Clyne, *Diamond Relat. Mater.*, 1997, **6**, 1612.
44 H. Windischmann and K. J. Gray, *Diamond Relat. Mater.*, 1995, **4**, 837.
45 M. J. Ulczynski, B. Wright and D. K. Reinhard, *Diamond Relat. Mater.*, 1998, **7**, 1639.

